Calculation of the Vibrationally Resolved Electronic Absorption Spectrum of the Propargyl Radical (H_2CCCH)

Wolfgang Eisfeld*

Theoretische Chemie, Department Chemie, Technische Universität München, D-85747 Garching, Germany

Received: November 18, 2005; In Final Form: January 9, 2006

The absorption spectrum of the propargyl radical in the region from 180 to 400 nm is investigated in detail by means of theory. Vertical excitation energies and potential energy surfaces are determined by highly accurate multireference configuration interaction (MRCI) calculations. The vibrational dynamics of several electronic states is studied, and line intensities and positions are calculated with respect to the electronic and vibrational ground state. Four electronic states absorb in the region of interest: $1\ ^2B_2$, $2\ ^2B_1$, $2\ ^2B_2$, and $3\ ^2B_1$. However, electronic excitations into the $^2B_2$ states are dipole-forbidden from the $\tilde{X}\ ^2B_1$ ground state and corresponding vibronically allowed transitions are shown to be weak. The spectrum is dominated by the strong $2\ ^2B_1 \leftarrow 1\ ^2B_1$ band which is computed in overall good agreement with available experiments. A strong absorption at 242 nm, which has been assigned to propargyl, is not confirmed by the calculations, and only very weak absorptions are found at wavelengths shorter than 280 nm. The present results strongly suggest that the 242 nm feature must be due to a different species.

I. Introduction

The propargyl radical (H_2CCCH), an open-shell system of considerable stability, has attracted the interest of many research groups over the last two decades. It is believed to play a significant role in combustion chemistry, particularly in the formation of polycyclic aromatic hydrocarbons (PAHs) and soot. Many experiments and theoretical studies were undertaken to elucidate the formation mechanisms, but the results seem somewhat controversial.[1−13] The formation by recombination of C_3H_3 radicals was first proposed by Wu and Kern in 1987.[1] Propargyl is also considered to play a significant role in the chemistry of hydrocarbon-rich planetary atmospheres and in the interstellar medium (see ref 14 and refs therein). However, it seems that it has not yet been detected in interstellar space.

Due to its significance in combustion, atmospheres, and astrochemistry, a considerable number of experiments were performed to gain insight into the spectroscopy and dynamics of this radical. The first electronic absorption spectrum was recorded by Ramsay and Thistlethwaite in 1966 and shows several diffuse signals between 345 and 290 nm.[15] This band system is due to the $2\ ^2B_1 \leftarrow \tilde{X}\ ^2B_1$ transition as was correctly assigned by the authors. A more detailed spectrum of this region was published recently together with the corresponding spectrum of the propargyl cation.[16] Further absorption spectra measured in the region between 280 and 370 nm agree quite well, although different precursors for the propargyl radical were utilized.[10,13] Thus, there is good evidence that H_2CCCH is the spectroscopic carrier of this band system.

In 1997, Fahr et al. published the first absorption spectrum of a second band, assigned to the $3\ ^2B_1 \leftarrow \tilde{X}\ ^2B_1$ transition.[17] They observed a strong, unstructured absorption in the region from 300 to 230 nm with a maximum at 242 nm. Deyerl et al. reproduced this absorption signal by action spectroscopy in their study of the photodissociation dynamics of the propargyl radical.[18] However, Giri et al.[13] did not observe such an absorption when starting from halogen-free precursors. This finding is in agreement with two earlier studies by Atkinson and Hudgens in which $C_3H_3Cl_2$ was proposed as the carrier of the strong absorption at 242 nm.[10,19] On the other hand, in a very recent study, Fahr and Laufer also observed an absorption in this region when propargyl radicals were produced by photodissociation of allene and propyne.[20] This finding cannot be due to halogenated compounds such as the ones suggested by Atkinson and Hudgens.

The propargyl radical was also studied by means of computational chemistry, though the theoretical literature is surprisingly sparse for a species of such general interest. The stability of different C_3H_3 isomers was studied extensively, and the propargyl radical was found to be the most stable structure.[21,22] The low-lying electronically excited states were investigated as well.[23,17] It was found that the lowest two excited states correspond to $^2B_2$ and $^2B_1$ state symmetries within the C_{2v} point group which reflects the symmetry of the ground-state equilibrium geometry. However, both states relax to geometries of C_s symmetry.[23] The transition to the lowest excited state, which is of $^2B_2$ symmetry, is dipole-forbidden because the ground-state wave function transforms like $^2B_1$. Thus, the second observed absorption band would have to be caused by a higher excited state. Fahr et al. calculated the vertical excitation energies of several higher electronic states of $^2B_1$ and $^2B_2$ symmetry and found that the next two states are $\tilde{C}\ ^2B_2$ and $\tilde{D}\ ^2B_1$.[17] However, the vertical excitation energy of the second dipole-allowed transition to the $\tilde{D}\ ^2B_1$ state corresponds to a wavelength of roughly 215 nm. Just recently, we studied the vertical excitation energies as well as the vertical and adiabatic ionization potentials of propargyl and three other C_3H_3 isomers.[24] The conclusion from this study is that neither the propargyl nor the other C_3H_3 radicals can be responsible for the strong absorption at 242 nm.

This interpretation is based on the vertical excitation energies in conjunction with the calculated electronic oscillator strengths. This fixed-nuclei picture does not take into account the

* E-mail: wolfgang.eisfeld@ch.tum.de.

10.1021/jp056683s CCC: $33.50
Published on Web 02/24/2006

possibility of transitions which only become allowed by vibronic coupling. To study such excitations, the vibrational dynamics has to be treated for all relevant states, which is the aim of the present study. It is also necessary to compute transition probabilities both for dipole-allowed transitions and for excitations which are only vibronically allowed. Furthermore, the simulation of vibrationally resolved absorption spectra can be used to directly compare the theoretical results to available experiments. In this way, the spectra can be interpreted and assigned based on the computational results.

II. Theoretical Model and Computational Details

The aim of this study is to obtain a vibrationally resolved absorption spectrum which accounts for both dipole-allowed and dipole-forbidden electronic transitions. To this end, a simple method is devised in which the potential V of the vibrational Hamiltonian, depending on the coordinates $\mathbf{q}$, is taken to be separable

$$V(\mathbf{q}) = \sum_{j=1}^{12} v_j(q_j) \tag{1}$$

Thus, the 12-dimensional (12D) problem reduces to twelve 1D problems which can easily be solved without being limited, for example, to the harmonic approximation. The latter is particularly important because the symmetry point group of the equilibrium geometry changes upon excitation, resulting in double-well potentials along certain modes (see below). The potential energy surfaces (PESs) of the investigated electronic states are calculated along the Cartesian normal-mode coordinates q_j obtained from electronic structure calculations. These data are fitted to simple expressions which provide the potential functions v_j for the 1D vibrational Hamiltonians. The 1D problems are solved by discrete variable representation (DVR) which results in vibrational energies and a grid representation of the corresponding nuclear wave functions ϕ_j. Since the 12D wave functions Φ are simple Hartree products of the 1D functions

$$\Phi(\mathbf{q}) = \prod_{j=1}^{12} \phi_j(q_j) \tag{2}$$

it is trivial to evaluate the Franck−Condon (FC) integrals by

$$\langle \Phi'' | \Phi' \rangle = \prod_{j=1}^{12} \langle \phi_j'' | \phi_j' \rangle \tag{3}$$

For the treatment of transitions which only become allowed by vibronic coupling, one has to go beyond the Condon approximation and compute Herzberg−Teller integrals. To this end, the transition dipole functions $\mu_j(q_j)$ are calculated along all nontotally symmetric modes and the 12D transition moment surface is expanded as

$$\mu(\mathbf{q}) = \mu_0 + \sum_{\substack{j=1 \\ \Gamma_{v_j} \neq A_1}} \mu_j(q_j) \tag{4}$$

The Herzberg−Teller integrals are obtained as[25]

$$\langle \Phi'' | \mu(\mathbf{q}) | \Phi' \rangle = \sum_{\substack{j=1 \\ \Gamma_{v_j} \neq A_1}} \langle \phi_j'' | \mu_j | \phi_j' \rangle \cdot \prod_{k \neq j} \langle \phi_j'' | \phi_j' \rangle \tag{5}$$

The method outlined above is based on the rather crude approximation of independent oscillators, which may warrant some justification. In principle, this is comparable to standard FC calculations, which are based on independent oscillators as well. To compute intensities, one would need to evaluate multidimensional integrals, and this quickly becomes unfeasible for larger molecules. However, within the harmonic approximation, the normal modes are obtained by coordinate transformations that delete all mode−mode couplings and thus yield independent oscillators by default. These normal modes in general are different for each electronic state but can be transformed into each other by the Duschinsky matrix. On this basis, it is easily possible to compute FC integrals accurately within the harmonic approximation.[26] This method cannot be applied in the present case because of anharmonicity, yielding pronounced double-well potentials along several modes. By the present method, one can easily describe the double-well potentials but the Duschinsky rotation of normal modes cannot be accounted for. Thus, accurate absorption frequencies are obtained only if the normal modes of the initial and final electronic states are very similar. In general, this will not be the case and the computed frequencies will not be very accurate. However, harmonic frequencies are often not very accurate either, and applying the harmonic approximation in the present case would introduce much larger, even qualitative, errors in the computation of intensities. Therefore, the present method is the best choice of an independent oscillator model for the problem treated in this study. Any improvement over this simple theory would require treatment of the full-, or at least higher-dimensional, nonseparable, anharmonic PESs or, in the normal-mode picture, explicit coupling of the normal modes.

To determine the necessary potential functions, one first has to obtain the normal-mode coordinates of the electronic ground state. These are computed at the density functional theory (DFT) level, utilizing the B3LYP functional and the correlation-consistent triple-ζ basis set augmented by diffuse functions (AVTZ). The Gaussian 03 program package was used for these calculations.[27]

Ground- and excited-state energies and properties are determined by the internally contracted multireference configuration interaction (MRCI) method.[28,29] The energies include the multireference version of the Davidson correction. The reference wave function is optimized by complete active space self-consistent field (CASSCF) calculations. The reference configuration space for the MRCI computations is the same as that for the CASSCF calculations. In the previous study, it turned out that a fairly small active space is sufficient to account for the static electron correlation of all electronic states of interest. Though several valence electrons are excluded from the active space, all of them are correlated in the single and double excitations to form the CI matrix. The active space for all calculations consists of one a_1, three b_1, four b_2, and one a_2 orbitals, containing five active electrons. Seven a_1 and one b_2 orbitals are inactive (i.e., always doubly occupied). The CASSCF wave function is averaged over one $^2A_1$, four $^2B_1$, three $^2B_2$, and one $^2A_2$ states.

The potential functions for the investigated electronic states are calculated with respect to the ground-state equilibrium geometry. Then the energies of ground and excited states are computed for distortions along the Cartesian normal-mode coordinates determined for the electronic ground state as stated above. The ground-state normal coordinates are used because all bands of the spectrum have this initial state in common and

TABLE 1: Harmonic Frequencies and Symmetry and Assignment of Corresponding Normal Modes Computed at the DFT B3LYP/AVTZ Level of Theory

		ω/cm^{-1}			
mode	symmetry	theory	experiment	ref	assignment
ν_1	a_1	3459.0	3308.5 ± 0.5	34	H−CC stretch
ν_2	a_1	3143.5	3028.3 ± 0.6	34	HCH symmetric stretch
ν_3	a_1	2008.7	1935.4 ± 0.4	34	HC−C stretch
ν_4	a_1	1460.1	1440.4 ± 0.5	34	HCH symmetric bend
ν_5	a_1	1089.6	1061.6 ± 0.8	34	H_2C−C stretch
ν_6	b_1	697.1	686.6 ± 0.4	34	HCH out-of-plane bend
ν_7	b_1	482.7	483.6 ± 0.5	34	HCC out-of-plane bend
ν_8	b_1	410.0	483.5	35	CCC out-of-plane bend
ν_9	b_2	3231.5	3109	36	HCH asymmetric stretch
ν_{10}	b_2	1033.8	1016.7 ± 0.4	34	HCH in-plane wagging
ν_{11}	b_2	637.5	620.0 ± 2.0	34	HCC in-plane bend
ν_{12}	b_2	356.0			CCC in-plane bend

because the initial state strongly determines the shape of the absorption spectra.

The accuracy of the vertical excitation energies is further improved by a simple exponential basis set extrapolation of reference and correlation energy as well as the Davidson correction.[24] For this extrapolation, the correlation-consistent basis sets of triple-, quadruple-, and quintuple-ζ quality, augmented by diffuse functions, were utilized. All MRCI calculations were performed by the Molpro program package.[30]

III. Results and Discussion

A. Potential Energy and Transition Dipole Surfaces. The equilibrium geometry of the electronic ground state of propargyl has been determined in several studies before at various theoretical levels.[22−24,31−33] The reference geometry used in the present study is described in detail in the previous paper (ref 24) and is not discussed here in detail. The main feature is that it is of C_{2v} symmetry with a linear arrangement of the three C atoms and a single H atom. The equilibrium geometries of the excited states are not explicitly optimized. Instead, the excited-state PESs are expanded around the ground-state equilibrium point along the ground-state normal-mode coordinates. The latter are obtained by a harmonic normal-mode analysis at the DFT level. The frequencies and normal modes obtained are summarized in Table 1.

The agreement of the frequencies with available experiments is fairly good and in accord with a very recent high-level study by Jochnowitz et al.[34] The lower frequencies up to roughly 1000 cm^{-1} all correspond to b_1 and b_2 modes which lower the symmetry of the system. The only nontotally symmetric high-frequency mode is due to the asymmetric H−C−H stretching vibration.

The normal-mode coordinates obtained from the DFT calculation are then utilized to determine the PESs of the ground and excited states. The three lowest states of $^2B_1$ symmetry and the two lowest states of $^2B_2$ symmetry are considered. From the work of Honjou et al.,[23] it is already known that the lowest two excited states exhibit minima with reduced symmetry of the nuclear frame. From the present calculations of cuts of the PESs, it becomes obvious that the other two excited states exhibit the same effect. This results in double-well potentials along the corresponding normal modes which is the reason the harmonic approximation is not suitable for the treatment of the current problem. This behavior is particularly pronounced along the q_{12} mode for which the PES cuts are depicted in Figure 1.

The q_{12} coordinate corresponds to the CCC in-plane bending mode of b_2 symmetry. The 2 $^2B_2$ and 3 $^2B_1$ states show pronounced double-wells along this mode with well-depths of 5190 and 5960 cm^{-1} respectively. This indicates that the equilibrium geometry of these two states should be distorted along this in-plane mode. According to a rough estimate, approximately 10 vibrational levels should be found below the barrier and thus an extended vibrational progression due to this mode must be expected. Figure 1 also shows that the two $^2B_2$ states come fairly close in energy near the double-well minima. At first glance, the existence of avoided crossings in that region cannot be ruled out. However, it is found by inspection of dipole and transition moments that no avoided crossing is present there. At higher energies, a conical intersection is observed between the 2 $^2B_2$ and the 3 $^2B_1$ states. Therefore, non-Born−Oppenheimer effects may play a role for the correct description of the dynamics, which are not accounted for in the present study.

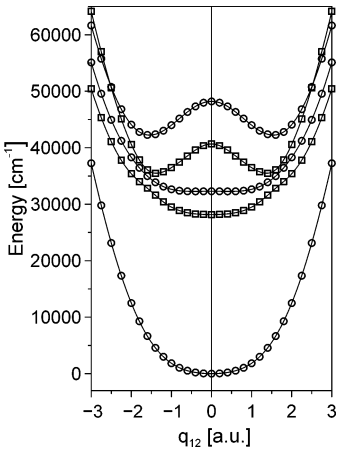

Figure 1. Potential energies of low-lying excited states along the q_{12} (b_2) mode: open circles, $^2B_1$ states; open squares, $^2B_2$ states.

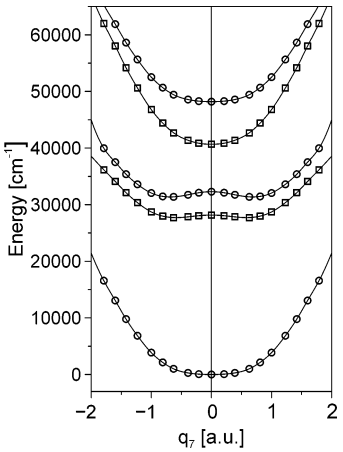

Figure 2. Potential energies of low-lying excited states along the q_7 (b_2) mode: open circles, $^2B_1$ states; open squares, $^2B_2$ states.

Double-wells are also observed along the q_7 coordinate which corresponds to the HCC out-of-plane bending vibration of b_1 symmetry. The respective PES cuts are shown in Figure 2.

In contrast to the PESs along q_{12}, the 2 $^2B_2$ and 3 $^2B_1$ states exhibit single minima at undisplaced geometries, while the 1 $^2B_2$ and 2 $^2B_1$ states have double-wells along q_7. This is in agreement with the calculations of Honjou et al.[23] who found equilibrium geometries for the latter two states which are distorted out of the molecular plane. However, the depths of the double-wells are much less than those observed for the higher two states along q_{12}. The barrier heights are only 450 and 930 cm^{-1}, respectively. Nevertheless, it is clear that the shape of these potentials will cause a significant vibrational structure in the absorption bands.

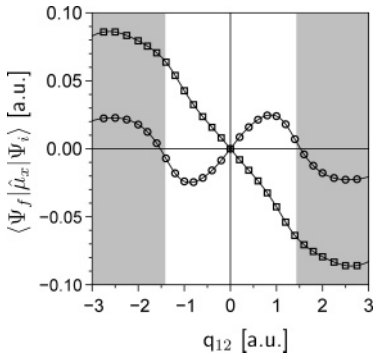

Figure 3. Transition dipole moments between the 1 $^2B_2$ (open circles) and 2 $^2B_2$ (open squares) states and the $^2B_1$ ground state along the q_{12} (b_2) mode. The shaded area indicates the region in which the nuclear wave function of the initial state is essentially zero.

To treat the vibronic absorption bands of dipole-forbidden electronic transitions, one has to go beyond the Condon approximation. The necessary transition dipole functions are calculated together with the potential energies of the excited states. However, only distortions along the nontotally symmetric modes result in nonzero transition moments for the $^2B_2 \leftarrow {}^2B_1$ excitations. The transition moment functions between the ground state and the two $^2B_2$ states are plotted along the particularly important q_{12} coordinate in Figure 3.

It is clear that both transition functions have to be antisymmetric, and often these functions are assumed to be linear. However, Figure 3 clearly shows that this would be a rather poor approximation at least for the 1 $^2B_2$ state. To calculate vibronic intensities, one needs the matrix elements of the transition function over the initial and final vibrational wave function. The initial vibrational wave function has a finite width because for larger displacements along the mode coordinate it becomes zero within numerical accuracy. Therefore, the transition function needs to be correctly represented only within the numerical quadrature limits. In Figure 3, the region in which the initial state wave function is essentially zero is indicated by the shaded area. Within the relevant region, the transition function for the 2 $^2B_2$ state is indeed nearly linear but the transition moment for the 1 $^2B_2$ state shows oscillatory behavior. Not only the shape of the PES but also that of the transition function have a significant influence on the intensities of the corresponding vibronic transitions.

B. Vibrationally Resolved Absorption Spectra. It is possible to analyze each band, belonging to a single electronic state, separately. In contrast, the experimental spectrum is a superposition of the single bands due to the proximity of the involved electronic states and the extended vibrational progressions. To simulate the observed spectrum, the absolute intensities of all transitions have to be used. This is achieved by computing both electronic oscillator strengths and vibrational transition intensities. In the following, the individual bands are analyzed first before the complete absorption spectrum is discussed. In all simulated spectra shown in the following, a Gaussian line broadening with fwhm = 100 cm^{-1} was applied to facilitate comparison to the experiments. The chosen value is slightly less than the line widths estimated from the spectrum by Wyss et al.[16] The initial state for all bands is the vibrational ground state, and thus, no hot bands are calculated. This situation can be compared to the Ne matrix spectrum at 5 K.

The 2 $^2B_1 \leftarrow 1\ ^2B_1$ transition is dipole-allowed, and a significant transition moment is calculated for this excitation.[24] As discussed above, the change in symmetry of the excited-state equilibrium geometry is expected to lead to pronounced vibrational dynamics. The calculated spectrum of this band, depicted in Figure 4, confirms this assumption.

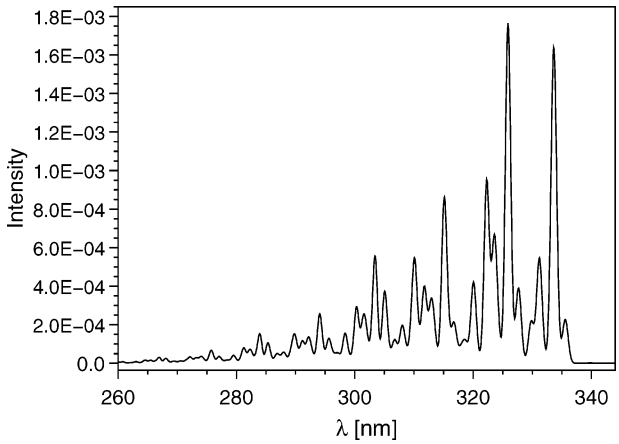

Figure 4. Simulation of the absorption band of the dipole-allowed 2 $^2B_1 \leftarrow 1\ ^2B_1$ transition.

The 0−0 transition, computed at a wavelength of 339.8 nm, is only weak and is not visible in the spectrum. The first observable line is found at 335.6 nm and is due to the 8_0^2 transition. It should be noted that the potential along q_8 is of double-well shape with a fairly low barrier to inversion. This is also true for q_7 and q_{12}. As a consequence, tunneling splitting occurs even for the lowest vibrational levels and the radical is nonrigid in the excited state. Therefore, the appropriate molecular symmetry to assign transitions is C_{2v} rather than C_s for both the initial and final states.[37] As a consequence of the effective C_{2v} symmetry and the symmetric double-wells, only even quanta of excitations are found to give nonzero intensities for the corresponding modes. Some of the discrepancies between the present assignments and those of Wyss et al. may be due to the use of C_s as the effective symmetry in ref 16.

The energy of the first observable peak is slightly higher (by 650 cm^{-1}) than the experimental 343.0 nm absorption which Wyss et al.[16] assigned to the 0−0 transition of this band. The two most intense peaks are computed for the 8_0^4 and $8_0^4\ 7_0^2$ transitions at 333.6 and 325.9 nm, respectively. The two next intense signals at 322.3 and 315.1 nm are due to $8_0^4\ 5_0^1$ and $8_0^4\ 7_0^2\ 5_0^1$ excitations. Several further lines with significant intensities result from progressions based on the higher excitations of modes ν_7 and ν_8. However, as is usually found for molecules larger than the simplest ones, most signals are composed of a number of transitions which are not resolved in the experiment. The assignments of the most intense lines are collected in Table 2.

The approximations applied in the present work do not allow us to match the experimental spectrum in all its features. However, the overall agreement is quite acceptable, and the calculation is good enough to give a general analysis of the vibrational progressions. Particularly, the width of the spectrum, stretching from roughly 340 to 280 nm, is reproduced very well. The present results confirm the interpretation of Wyss et al. that ν_5 and ν_8 are among the most active modes in the vibrational dynamics of this band. The assignment of strong signals to the excitations of ν_6 are not in agreement with the calculations which instead indicate that mode ν_7 plays an important role. Also, several assignments of transitions involving odd quanta in ν_8 and ν_6 seem unlikely. Such transitions can only be caused by non-Condon effects as they are treated for the dipole-forbidden transitions in the present study. Their intensities are much lower than transitions with even quanta if the transition moment at

TABLE 2: Energies, Excitation Wavelengths, and Assignments of Vibronic Transitions of the Calculated 2 $^2B_1$ ← 1 $^2B_1$ Band

energy/cm^{-1}	λ/nm	assignment
29799.4	335.6	8_0^2
29972.5	333.6	8_0^4
30194.5	331.2	8_0^6
30320.2	329.8	$12_0^2\ 8_0^4$
30511.0	327.8	$8_0^2\ 7_0^2$
30684.1	325.9	$8_0^4\ 7_0^2$
30906.2	323.6	$8_0^6\ 7_0^2$
31025.7	322.3	$8_0^4\ 5_0^1$
31031.8	322.3	$12_0^2\ 8_0^4\ 7_0^2$
31247.7	320.0	$8_0^6\ 5_0^1$
31687.0	315.6	$8_0^4\ 7_0^4$
31737.3	315.1	$8_0^4\ 7_0^2\ 5_0^1$
31959.3	312.9	$8_0^6\ 7_0^2\ 5_0^1$
32073.6	311.8	$8_0^4\ 5_0^2$
32241.7	310.2	$8_0^4\ 3_0^1$
32463.7	308.0	$8_0^6\ 3_0^3$
32785.2	305.0	$8_0^4\ 7_0^2\ 5_0^2$
32953.3	303.5	$8_0^4\ 7_0^2\ 3_0^1$
33175.3	301.4	$8_0^6\ 7_0^2\ 3_0^1$
33294.8	300.3	$8_0^4\ 5_0^1\ 3_0^1$
34006.4	294.1	$8_0^4\ 7_0^2\ 5_0^1\ 3_0^1$
35212.1	284.0	$8_0^4\ 7_0^2\ 3_0^2$

the vertical excitation point, μ_0, is significant, which is the situation here. Clearly, a much more sophisticated treatment of the vibrational dynamics is required for a more detailed assignment of the experimental peaks which is, however, beyond the scope of the present study.

The 3 $^2B_1$ ← 1 $^2B_1$ transition is also dipole-allowed, but a much lower oscillator strength is computed for this electronic excitation (1.15×10^{-3} vs 1.31×10^{-2}). From the strong geometrical change upon excitation, which is obvious from Figure 1, a very strong vibrational activity is expected. This is confirmed by the calculated spectrum shown in Figure 5.

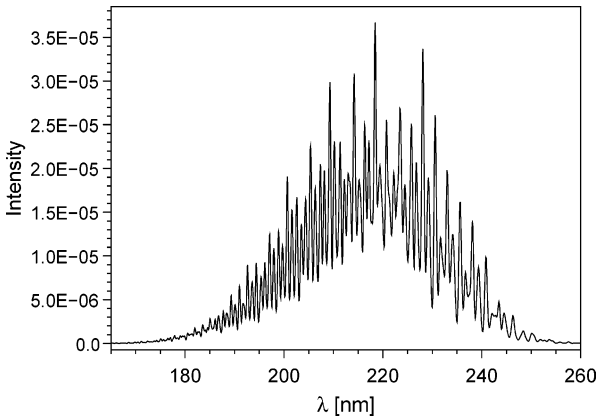

Figure 5. Simulation of the absorption band of the dipole-allowed 3 $^2B_1$ ← 1 $^2B_1$ transition.

The band roughly stretches from 165 to 260 nm, and the oscillator strength is distributed over more than 4000 single transitions. As a result of the deep double-well potential along q_{12}, the first discernible feature at 257.6 nm already corresponds to the $8_0^2\ 12_0^{12}$ transition. The 0−0 transition would correspond to a wavelength of 293.3 nm, but the computed intensity of this line is numerically zero. The most intense peak at 218.4 nm is due to the $3_0^2\ 8_0^2\ 11_0^4\ 12_0^{16}$ excitation, and two further strong signals belong to the same progression in the ν_3 mode ($3_0^1\ 8_0^2\ 11_0^4\ 12_0^{16}$ at 228.1 nm and $3_0^3\ 8_0^2\ 11_0^4\ 12_0^{16}$ at 209.3 nm, respectively). It is found throughout the spectrum that the most active modes are ν_{12}, ν_{11}, ν_8, ν_5, and ν_3 with particularly high excitations in ν_{12}. The calculated vertical excitation energy corresponds to 206.1 nm which is somewhat higher in energy than the estimated maximum of the band envelope at about 220 nm. The most intense transition calculated for vertical excitation at 206.1 nm corresponds to $3_0^2\ 5_0^3\ 8_0^2\ 11_0^4\ 12_0^{16}$.

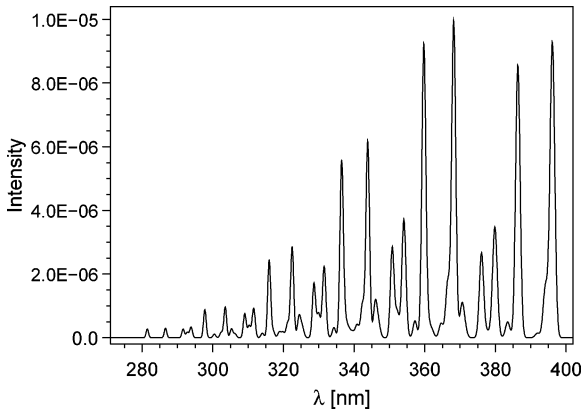

Figure 6. Simulation of the absorption band of the dipole-forbidden 1 $^2B_2$ ← 1 $^2B_1$ transition.

The lowest excited state of propargyl is of $^2B_2$ symmetry, but the electronic transition 1 $^2B_2$ ← 1 $^2B_1$ is dipole-forbidden. Nevertheless, transitions become allowed by vibronic coupling. Therefore, weak signals on the red side of the experimentally observed band have been interpreted as dipole-forbidden but vibronically allowed transitions to the 1 $^2B_2$ state.[16] The selection rule for allowed vibronic transitions is $\Gamma_f \otimes \Gamma_{\hat{\mu}} \otimes \Gamma_\nu \otimes \Gamma_i \supset \Gamma_{A_1}$, where Γ denotes the irreducible representation of the nuclear point group, indices *i* and *f* indicate the initial and final electronic states, respectively, $\hat{\mu}$ is the dipole transition operator, and ν stands for the final vibrational state. The initial vibrational state is assumed to be the ground state and thus is totally symmetric (A_1). The irreducible representations of the three components of the dipole operator in C_{2v} are A_1, B_1, and B_2, and thus, one easily finds that Γ_ν must be either B_1 or B_2. In the present work, such vibronic transitions and the corresponding line intensities are calculated explicitly and the selection rules can be used to check those results. To this end, the coordinate-dependent dipole transition functions are taken into account in the computation of the transition probabilities. The resulting spectrum of the 1 $^2B_2$ ← 1 $^2B_1$ band is depicted in Figure 6.

The spectrum shows a series of well-resolved peaks between 280 and 400 nm, and several patterns can be recognized. There are two series of pairs of lines which both show a fairly regular progression. The first two intense peaks are due to the 7_0^1 and 11_0^1 transitions, respectively. The weak shoulder on the blue side of the first peak is caused by the 12_0^1 transition which, however, has much lower intensity. The progression based on the first two strong signals originates from excitation of mode ν_3. A less intense progression is seen for a pair of peaks at slightly shorter wavelengths (379.9 and 376.1 nm, respectively). These signals correspond to the 7_0^3 and $7_0^2\ 11_0^1$ transitions, respectively. Two more transitions, $7_0^1\ 6_0^2$ and $7_0^1\ 5_0^1$, contribute to the peak at lower energy but are weaker, and these signals are not resolved. The progression based on these two peaks is also caused by excitations of mode ν_3 which results in the second regular progression. The assignments and calculated state energies are collected in Table 3.

Wyss et al. assigned some weak features of their experimental spectrum to a progression in mode ν_8 of the 1 $^2B_2$ ← 1 $^2B_1$

TABLE 3: Energies, Excitation Wavelengths, and Assignments of Vibronic Transitions of the Calculated 1 $^2B_2 \leftarrow 1\ ^2B_1$ Band

energy/cm^{-1}	λ/nm	assignment
25244.8	396.1	7_0^1
25883.3	386.3	11_0^1
26320.8	379.9	7_0^3
26591.4	376.1	$7_0^2\ 11_0^1$
27159.9	368.2	$7_0^1\ 3_0^1$
27798.4	359.7	$11_0^1\ 3_0^1$
28235.9	354.2	$7_0^3\ 3_0^1$
28506.5	350.8	$7_0^2\ 11_0^1\ 3_0^1$
29082.1	343.9	$7_0^1\ 3_0^2$
29720.6	336.5	$11_0^1\ 3_0^2$
30158.0	331.6	$7_0^3\ 3_0^2$
30428.7	328.6	$7_0^2\ 11_0^1\ 3_0^2$
31011.4	322.5	$7_0^1\ 3_0^3$
31649.8	316.0	$11_0^1\ 3_0^3$
32087.3	311.6	$7_0^3\ 3_0^3$
32357.9	309.0	$7_0^2\ 11_0^1\ 3_0^3$
32947.6	303.5	$7_0^1\ 3_0^4$
33586.1	297.7	$11_0^1\ 3_0^4$
34023.6	293.9	$7_0^3\ 3_0^4$
34294.2	291.6	$7_0^2\ 11_0^1\ 3_0^4$
34891.0	286.6	$7_0^1\ 3_0^5$
35529.5	281.5	$11_0^1\ 3_0^5$

band.[16] The interpretation of two peaks being caused by the 0−0 and 8_0^2 transitions is rather unlikely according to the vibronic selection rules discussed above. A final state of this band must have odd quanta in either a b_1 or a b_2 mode to be observable. The calculation also indicates that a more extended progression should be visible, particularly at lower energy than the observed signals. This seems not to be consistent with the experimental findings. Thus, the present calculations give no support of the assignment of weak features to vibronic transitions into the 1 $^2B_2$ electronic state.

Besides the observed and confirmed 2 $^2B_1 \leftarrow 1\ ^2B_1$ band system, a further strong absorption with a maximum at 242 nm has been discussed in the literature.[17,18,20] At first, this feature has been assigned to the 3 $^2B_1$ state. However, the calculations of the present study confirm the previous theoretical work[24] that showed this state to be too high in energy to be responsible for the observed spectrum. The corresponding band depicted in Figure 5 has its maximum around 220 nm and thus cannot be responsible for the observation. In contrast, the calculated vertical excitation energy of the 2 $^2B_2$ state corresponds to 243 nm and thus would fit to the measurement. In the previous investigation, this assignment was ruled out because the 2 $^2B_2 \leftarrow 1\ ^2B_1$ transition is dipole-forbidden and transitions which only become allowed by vibronic coupling are usually weak. This assumption is investigated here by the explicit calculation of the vibronic spectrum of the 3 $^2B_2 \leftarrow 1\ ^2B_1$ band, which is shown in Figure 7.

The band stretches from roughly 205 to 310 nm and is rather congested, comparable to the 2 $^2B_1 \leftarrow 1\ ^2B_1$ band. However, the number of single transitions (roughly 800) which contribute to this dipole-forbidden feature is much lower than in the band of the 3 $^2B_1$ state. This is an effect of the stricter selection rules for dipole-forbidden but vibronically allowed transitions. The congestion of the band results from the strong geometrical change in the excited state which already became apparent from Figure 1. Therefore, all observable vibronic states are highly excited in mode ν_{12}. The first visible peak at 309.6 nm is due to the $12_0^8\ 11_0^1$ transition, while the unobservable 0−0 excitation would correspond to 344.4 nm. The most intense line is found at 255.5 nm and belongs to the $12_0^{12}\ 11_0^4\ 8_0^2\ 7_0^1\ 3_0^1$ transition. The most active modes are ν_{12}, ν_{11}, ν_8, ν_4, and ν_3. This is similar to the situation in the 3 $^2B_1$ state with the only difference that the ν_4 mode replaces ν_5 as an active mode.

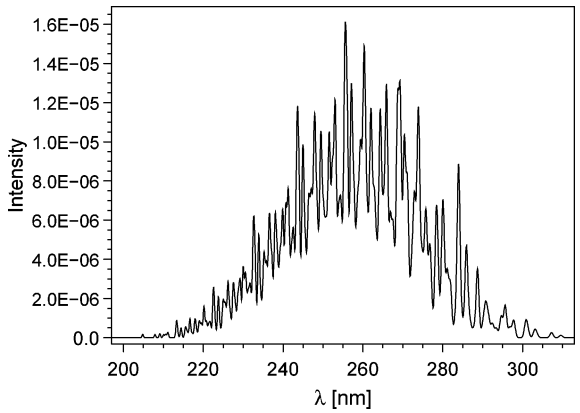

Figure 7. Simulation of the absorption band of the dipole-forbidden 2 $^2B_2 \leftarrow 1\ ^2B_1$ transition.

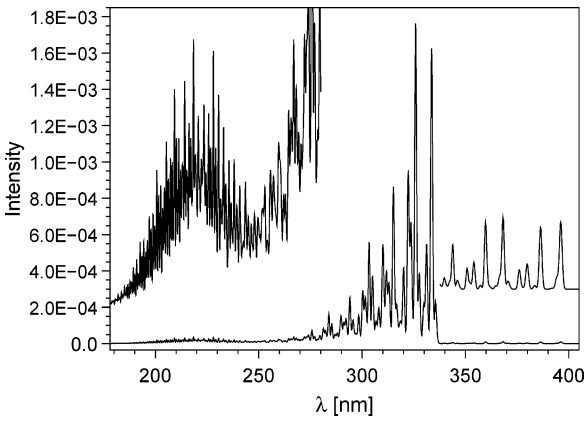

Figure 8. Simulation of the full absorption spectrum in the region from 400 to 180 nm. The additional traces from 280 to 180 nm and 400 to 340 nm are magnified by a factor of 40.

The maximum of the band envelope is found around 250−260 nm which is slightly longer than the vertical excitation and the experimental observation. The energy difference between the calculated band maximum and the experimental measurement is approximately 2000 cm^{-1} which is significantly more than the expected accuracy of the applied electronic structure methods. Even more striking is the comparison of the calculated intensities of all four bands which are combined to a complete spectrum in Figure 8.

At first glance it becomes apparent that the full spectrum is dominated by the 2 $^2B_1 \leftarrow 1\ ^2B_1$ band with its strong signals between 340 and 280 nm. Some very weak features can be noticed between 400 and 340 nm which are about 2 orders of magnitude less intense than the strongest absorptions of the full spectrum. These weak transitions are due to the electronically forbidden excitation to the 1 $^2B_2$ state which have been discussed by Wyss et al.[16] A second trace in Figure 8 shows this region magnified by a factor of 40. The tiny peak at the high-energy edge of the enlarged trace is found at 339.8 nm and is caused by the 0−0 transition to the 2 $^2B_1$ state. The significantly stronger second signal at 343.9 nm belongs to the $7_0^1\ 3_0^2$ transition into the 1 $^2B_2$ state and coincides very closely with an observed feature that was assigned to the 0−0 transition into this electronic state. However, based on the present calculations, it seems very unlikely that these dipole-forbidden but vibronically allowed excitations are observed in the experimental

spectrum. The computed intensity ratio between the lines of the $2\ ^2B_1 \leftarrow 1\ ^2B_1$ and the $1\ ^2B_2 \leftarrow 1\ ^2B_1$ bands is approximately an order of magnitude smaller than the one observed experimentally. Furthermore, there are a number of additional lines of similar or larger intensity due to the $1\ ^2B_2$ state which are not seen in the measurement. The question of the origin of the observed lines around 343 nm cannot be answered with certainty because the applied approximations in the calculation of the vibrational dynamics are too crude to achieve an accurate line-by-line match. A much more sophisticated calculation would be needed to obtain sufficiently precise energy levels and intensities.

In contrast, the method is good enough to answer another question with confidence. The computed spectrum shows clearly that no strong absorption is present in the region around 242 nm. Thus, the experimentally observed signal in this region, which was attributed to propargyl, must be due to a different species. In fact, this result is in agreement with the spectra of Wyss et al., which do not show any strong absorptions in the region between 280 and 240 nm either.[16] A careful inspection of the spectrum around 220 nm shows a broad absorption which is very weak compared to the dominant $2\ ^2B_1 \leftarrow 1\ ^2B_1$ band. The region between 280 and 180 nm is enlarged by a factor of 40 and depicted in a second trace in Figure 8. In the enlarged spectrum, the $3\ ^2B_1 \leftarrow 1\ ^2B_1$ band becomes recognizable as a broad absorption between 250 and 180 nm. In contrast, the $2\ ^2B_2 \leftarrow 1\ ^2B_1$ band, which would be expected to be visible between 300 and 220 nm, cannot be distinguished. Instead, the weak tail of the $2\ ^2B_1 \leftarrow 1\ ^2B_1$ band is superimposed in this region, and these dipole-allowed transitions are much stronger despite their small Franck−Condon factors. Thus, propargyl absorbs around 242 nm but only extremely weakly.

Both the present theoretical study and the experiment by Wyss et al. clearly contradict the interpretations by Fahr et al.[17,20] and Deyerl et al.,[18] assigning a strong absorption at 242 nm to propargyl. Thus, the question arises, what is the carrier of the 242 nm absorption? A survey of the literature yields that doubts about the origin of this signal have been published before. Only two years after the original assignment by Fahr et al.,[17] Atkinson and Hudgens published two articles which provided some evidence that under certain experimental conditions a signal at 242 nm is caused by the chlorine adduct to the propargyl radical, $C_3H_3Cl_2$.[10,19] This chlorine product was produced in an independent way, and an absorption spectrum in close agreement to that of Fahr et al. was recorded. In contrast, generating propargyl radicals by photodissociation of propyne or allene did not yield a strong absorption at 242 nm. In recent experiments by Giri et al.,[13] additional evidence was obtained for this finding. When propargyl was produced from a different halogen-free precursor (dipropargyl oxalate), the absorption in question was not found but the signal was obtained when propargyl chloride was used. However, it turns out that this chlorine adduct can only explain the experiments partially. In a very recent study, Fahr and Laufer measured a strong signal at 242 nm although the propargyl radicals were produced by the photodissociation of propyne, allene, and 2-butyne. Therefore, the adduct $C_3H_2Cl_2$ cannot be responsible for the feature in this experiment since no chlorine has been present in the system. It is not clear why photodissociation of the same precursors gives a strong signal in one experiment[20] while it does not in another.[10] The formation of propargyl in both experiments, which is identified by the $2\ ^2B_1 \leftarrow 1\ ^2B_1$ absorption, is out of the question. But the absence of the 242 nm feature in one of the two experiments clearly shows that propargyl cannot be the spectral carrier of this absorption. This interpretation is also supported by the present calculations and the spectrum of Wyss at al. which shows no absorption in the region of interest either. In the previous investigation, it was also shown that other C_3H_3 isomers are certainly not the carrier of this spectral signature.[24] The most likely interpretation is that another photofragment is responsible for the absorption. One obvious possibility would be vinylidene carbene (H_2CCC) which absorbs strongly in the region from 213 to 259 nm.[38−40] This has also been discussed by Atkinson and Hudgens. The spectrum of H_2CCC is rather characteristic in the region of interest, and therefore, it should be possible to verify this assumption if an experiment with sufficient resolution is carried out. In any case, recent experiments in which the absorption in question was utilized to study the photodynamics of propargyl radicals have to be reinterpreted.[18,41]

IV. Conclusions

In the present study, the absorption spectrum of the propargyl radical has been studied in detail. The energies of several electronic states have been determined with high accuracy by large-scale MRCI calculations. At the same theoretical level, 12D PESs of the three lowest $^2B_1$ and two lowest $^2B_2$ states have been computed along the normal-mode coordinates of the electronic ground state. A simple model is applied in which the PESs are represented as sums of 1D potential functions and all coupling terms are ignored. The 1D functions fully account for anharmonicity effects, which are important because the excited states show pronounced double-well potentials along several modes. The vibrational dynamics of all the states has been treated by a time-independent DVR method which yields vibrational state energies and nuclear wave functions. The wave functions have been used to compute the transition probabilities and line intensities for absorption from the electronic and vibrational ground states. The intensities of electronic dipole-forbidden but vibronically allowed transitions have been calculated by explicitly taking the coordinate dependence of the transition dipole moment into account. In this way, the dipole-allowed $^2B_1 \leftarrow \tilde{X}\ ^2B_1$ and dipole-forbidden $^2B_2 \leftarrow \tilde{X}\ ^2B_1$ bands have been treated on an equal footing.

The analysis of the single band systems shows that the band corresponding to the $2\ ^2B_1$ state is computed in good agreement with available experiments. The assignment of fairly strong, experimentally observed absorptions between 340 and 280 nm to this state is confirmed by the present investigation. A transition at 335.6 nm is computed for the first intense peak of the band, which is only 650 cm^{-1} higher in energy than the experimental observation. This is an excellent agreement, taking into account the difficulties to accurately calculate electronically excited states and also considering the applied approximations in the representation of the PESs. However, the first strong line does not correspond to the 0−0 transition, as assigned in the experimental spectra, but is due to the 8_0^2 excitation. The analysis also shows that most peaks of the spectrum are caused by more than one transition. Thus, a correct assignment of band systems of such complexity seems virtually impossible without theoretical calculations such as those presented here. On the other hand, a less approximate theoretical treatment of the vibrational dynamics is required to obtain a line-by-line match with experiment. Unfortunately, this is still not possible except for very small molecular systems.

The calculation of the remaining three bands in question shows the importance of treating line intensities on an equal footing. It turns out that the dipole-allowed $3\ ^2B_1 \leftarrow 1\ ^2B_1$ band

and both dipole-forbidden bands are of similar intensity, but all absorb about 2 orders of magnitude weaker than the 2 $^2B_1$ state. Due to this finding, the assignment of weak features to the red side of the confirmed 2 $^2B_1$ band to the 1 $^2B_2$ state seems unlikely. Besides the very low intensity, the calculation also yields several additional lines for this dipole-forbidden band which are not found in the experiment. For wavelengths shorter than 280 nm, the calculations show only very weak signals. The 3 $^2B_1 \leftarrow 1\ ^2B_1$ band can be recognized as a weak, broad absorption consisting of several thousand single transitions. The maximum of the band envelope is found around 220 nm. In contrast, the very weak signature of the 2 $^2B_2$ state cannot be distinguished because it is superimposed by features of the tail of the much stronger 2 $^2B_1 \leftarrow 1\ ^2B_1$ band. This finding gives clear evidence that an experimentally observed strong absorption at 242 nm cannot be caused by the propargyl radical. As a consequence, recent experimental observations based on this assignment need to be reinterpreted. The true carrier of the 242 nm absorption is not yet known with certainty. There is strong evidence that in some of the experiments the signal was caused by a chlorine adduct of the propargyl radical ($C_3H_3Cl_2$). Another absorber may be vinylidene carbene (H_2CCC) which is a known photofragment of propargyl.

Acknowledgment. The Deutsche Forschungsgemeinschaft is gratefully acknowledged for financial support. The author thanks Professor Wolfgang Domcke for many fruitful discussions and Dr. Andreas Markmann for his helpful comments on the manuscript. Large amounts of computing time have been provided by the Leibniz-Rechenzentrum.

References and Notes

(1) Wu, C. H.; Kern, R. D. *J. Phys. Chem.* **1987**, *91*, 6291−6296.

(2) Kern, R. D.; Singh, H. J.; Wu, C. H. *Int. J. Chem. Kinet.* **1988**, *20*, 731.

(3) Westmoreland, P. R.; Dean, A. M.; Howard, J. B.; Longwell, J. P. *J. Phys. Chem.* **1989**, *93*, 8171−8180.

(4) Alkemade, U.; Homann, K. *Z. Phys. Chem. Neue Folge* **1989**, *161*, 19.

(5) Hidaka, Y.; Nakamura, T.; Miyauchi, A.; Shiraishi, T.; Kawano, H. *Int. J. Chem. Kinet.* **1989**, *20*, 643.

(6) Miller, J. A.; Melius, C. F. *Combust. Flame* **1992**, *91*, 21−39.

(7) Morter, C. L.; Farhat, S. K.; Adamson, J. D.; Glass, G. P.; Curl, R. F. *J. Phys. Chem.* **1994**, *98*, 7029−7035.

(8) Kern, R. D.; Chen, H.; Kiefer, J. H.; Mudipalli, P. S. *Combust. Flame* **1995**, *100*, 177−184.

(9) Miller, J. A.; Volponi, J. V.; Pauwels, J.-F. *Combust. Flame* **1996**, *105*, 451.

(10) Atkinson, D. B.; Hudgens, J. W. *J. Phys. Chem. A* **1999**, *103*, 4242−4252.

(11) Howe, P.-T.; Fahr, A. *J. Phys. Chem. A* **2003**, *107*, 9603−9610.

(12) Miller, J. A.; Klippenstein, S. J. *J. Phys. Chem. A* **2003**, *107*, 7783−7799.

(13) Giri, B. R.; Hippler, H.; Olzmann, M.; Unterreiner, A. N. *Phys. Chem. Chem. Phys.* **2003**, *5*, 4641−4646.

(14) Le, T. N.; yu Lee, H.; Mebel, A. M.; Kaiser, R. I. *J. Phys. Chem. A* **2001**, *105*, 1847−1856.

(15) Ramsay, D. A.; Thistlethwaite, P. *Can. J. Phys.* **1966**, *44*, 1381−1386.

(16) Wyss, M.; Riaplov, E.; Maier, J. P. *J. Chem. Phys.* **2001**, *114*, 10355−10361.

(17) Fahr, A.; Hassanzadeh, P.; Laszlo, B.; Huie, R. E. *Chem. Phys.* **1997**, *215*, 59−66.

(18) Deyerl, H.-J.; Fischer, I.; Chen, P. *J. Chem. Phys.* **1999**, *111*, 3441−3448.

(19) Atkinson, D. B.; Hudgens, J. W. *J. Phys. Chem. A* **1999**, *103*, 7978−7989.

(20) Fahr, A.; Laufer, A. H. *J. Phys. Chem. A* **2005**, *109*, 2534−2539.

(21) Collin, G. J.; Desauriers, H.; De Maré, G. R.; Poirier, R. A. *J. Phys. Chem.* **1990**, *94*, 134−141.

(22) Vereecken, L.; Pierloot, K.; Peeters, J. *J. Chem. Phys.* **1998**, *108*, 1068−1080.

(23) Honjou, H.; Yoshimine, M.; Pacansky, J. *J. Phys. Chem.* **1987**, *91*, 4455−4459.

(24) Eisfeld, W. *Phys. Chem. Chem. Phys.* **2005**, *7*, 3924−3932.

(25) Eisfeld, W. *J. Chem. Phys.* **2004**, *120*, 6056−6063.

(26) Sharp, T. E.; Rosenstock, H. M. *J. Chem. Phys.* **1964**, *41*, 3453−3463.

(27) Frisch, M. J.; Trucks, G. W.; Schlegel, H. B.; Scuseria, G. E.; Robb, M. A.; Cheeseman, J. R.; Montgomery, J. A., Jr.; Vreven, T.; Kudin, K. N.; Burant, J. C.; Millam, J. M.; Iyengar, S. S.; Tomasi, J.; Barone, V.; Mennucci, B.; Cossi, M.; Scalmani, G.; Rega, N.; Petersson, G. A.; Nakatsuji, H.; Hada, M.; Ehara, M.; Toyota, K.; Fukuda, R.; Hasegawa, J.; Ishida, M.; Nakajima, T.; Honda, Y.; Kitao, O.; Nakai, H.; Klene, M.; Li, X.; Knox, J. E.; Hratchian, H. P.; Cross, J. B.; Bakken, V.; Adamo, C.; Jaramillo, J.; Gomperts, R.; Stratmann, R. E.; Yazyev, O.; Austin, A. J.; Cammi, R.; Pomelli, C.; Ochterski, J. W.; Ayala, P. Y.; Morokuma, K.; Voth, G. A.; Salvador, P.; Dannenberg, J. J.; Zakrzewski, V. G.; Dapprich, S.; Daniels, A. D.; Strain, M. C.; Farkas, O.; Malick, D. K.; Rabuck, A. D.; Raghavachari, K.; Foresman, J. B.; Ortiz, J. V.; Cui, Q.; Baboul, A. G.; Clifford, S.; Cioslowski, J.; Stefanov, B. B.; Liu, G.; Liashenko, A.; Piskorz, P.; Komaromi, I.; Martin, R. L.; Fox, D. J.; Keith, T.; Al-Laham, M. A.; Peng, C. Y.; Nanayakkara, A.; Challacombe, M.; Gill, P. M. W.; Johnson, B.; Chen, W.; Wong, M. W.; Gonzalez, C.; Pople, J. A. *Gaussian 03*, revision C.02; Gaussian, Inc.: Wallingford, CT, 2004.

(28) Werner, H.-J.; Knowles, P. J. *J. Chem. Phys.* **1988**, *89*, 5803.

(29) Knowles, P. J.; Werner, H.-J. *Chem. Phys. Lett.* **1988**, *145*, 514.

(30) MOLPRO is a package of ab initio programs written by H.-J. Werner and P. J. Knowles, with contributions from R. D. Amos, A. Berning, D. L. Cooper, M. J. O. Deegan, A. J. Dobbyn, F. Eckert, C. Hampel, G. Hetzer, T. Leininger, R. Lindh, A. W. Lloyd, W. Meyer, M. E. Mura, A. Nicklass, P. Palmieri, K. Peterson, R. Pitzer, P. Pulay, G. Rauhut, M. Schütz, H. Stoll, A. J. Stone, and T. Thorsteinsson.

(31) Botschwina, P.; Horn, M.; Flügge, J.; Seeger, S. *J. Chem. Soc., Faraday Trans.* **1993**, *89*, 2219−2230.

(32) Botschwina, P.; Oswald, R.; Flügge, J.; Horn, M. *Z. Phys. Chem.* **1995**, *188*, 29.

(33) Botschwina, P.; Horn, M.; Oswald, R.; Schmatz, S. *J. Electron Spectrosc.* **2000**, *108*, 109−122.

(34) Jochnowitz, E. B.; Zhang, Z.; Nimlos, M. R.; Varner, M. E.; Stanton, J. F.; Ellison, G. B. *J. Phys. Chem. A* **2005**, *109*, 3812−3821.

(35) Huang, J. W.; Graham, W. R. M. *J. Chem. Phys.* **1990**, *93*, 1583−1596.

(36) Jacox, M. E.; Milligan, D. E. *Chem. Phys.* **1974**, *4*, 45−61.

(37) Bunker, P. R.; Jensen, P. *Fundamentals of Molecular Symmetry*; Institute of Physics Publishing: Philadelphia, PA, 2005.

(38) Stanton, J. F.; DePinto, J. T.; Seburg, R. A.; Hodges, J. A.; McMahon, R. J. *J. Am. Chem. Soc.* **1997**, *119*, 429−430.

(39) Seburg, R. A.; Patterson, E. V.; Stanton, J. F.; McMahon, R. J. *J. Am. Chem. Soc.* **1997**, *119*, 5847−5856.

(40) Hodges, J. A.; McMahon, R. J.; Sattelmeyer, K. W.; Stanton, J. F. *Astrophys. J.* **2000**, *544*, 838−842.

(41) Zierhut, M.; Noller, B.; Schultz, T.; Fischer, I. *J. Chem. Phys.* **2005**, *122*, 094302.